High-Throughput Screening $MgFe_6Ge_6$-Prototype Bilayer Kagome Family

Lan-Ting Shi(师兰婷)[1,2,3,4†], Jian-Guo Si(司建国)[4†], Hui-Bin Zhou(周慧斌)[1,2], Xian-Biao Shi(石贤彪)[1,2], Peng-Fei Liu(刘鹏飞)[1,2], Le-De Xian(冼乐德)[3,4], Ping Zhang(张平)[5,6], and Bao-Tian Wang(王保田)[1,2,7*]

[1]*Institute of High Energy Physics, Chinese Academy of Science, Beijing 100049, China*
[2]*Spallation Neutron Source Science Center, Dongguan 523803, China*
[3]*Tsientang Institute for Advanced Study, Zhejiang 310024, China*
[4]*Songshan-Lake Materials Laboratory, Dongguan 523808, China*
[5]*Institute of Applied Physics and Computational Mathematics, Beijing 100088, China*
[6]*School of Physics and Physical Engineering, Qufu Normal University, Qufu 273165, China*
[7]*Collaborative Innovation Center of Extreme Optics, Shanxi University, Taiyuan 030006, China*

(Received 27 October 2025; accepted manuscript online 27 January 2026)

Kagome materials host intertwined phenomena, including nontrivial band topology, superconductivity, and complex charge-density-wave order, making them an important platform in condensed-matter physics and materials science. Motivated by extensive studies on the AV_3Sb_5 family of materials, we perform high-throughput first-principles calculations to screen bilayer kagome AM_6X_6 compounds with an $MgFe_6Ge_6$-prototype structure as potential weak-coupling superconductors. Thereafter, we systematically evaluate the thermodynamic, dynamic, and magnetic stabilities, followed by electron–phonon coupling (EPC) calculations and superconducting transition temperature estimates based on the Allen–Dynes-modified McMillan equation. From 168 candidates, we identify 31 weak-coupling superconductors that satisfy both the thermodynamic and dynamical stability criteria in our screening workflow. Focusing on compounds without partially filled f shells, we obtain superconducting transition temperatures (T_c) of 0.65–3.97 K with EPC constants $\lambda = 0.37$–0.62, indicating conventional weak-coupling superconductivity. The EPC is typically driven by vibrations within the kagome layers, with Sn-containing materials exhibiting low-frequency soft modes that contribute significantly to λ. By providing a global mapping of stability and weak-coupling superconductivity in bilayer kagome AM_6X_6 compounds, this study offers a practical theoretical database and design principles for future experimental exploration.

DOI: 10.1088/0256-307X/43/3/030711 CSTR: 32039.14.0256-307X.43.3.030711

Introduction. The study of geometrically frustrated atomic arrangements has become a cornerstone of condensed matter physics owing to their ability to generate a wide array of fascinating and unconventional physical properties. Among the most prominent examples is the kagome lattice, a distinctive structure characterized by a network of corner-sharing triangles.[1] Materials with kagome layers provide a unique platform for exploring the intricate interactions between lattice geometry, magnetic ordering, and electronic structures.[2] Notable topologically nontrivial states in kagome materials have been associated with emergent electronic phenomena, including Dirac points, van Hove singularities, and geometry-induced flat bands.[3–8] Furthermore, kagome materials are recognized for their diverse quantum properties, such as frustrated magnetism,[9–11] anomalous Hall effect,[12–16] charge-density-wave (CDW) order,[17–20] and unconventional superconductivity.[21–27] Consequently, identifying kagome-based compounds can significantly advance condensed matter and material physics by providing new pathways for exploring complex quantum states.

In kagome materials, typical systems are the AV_3Sb_5 (A = K, Rb, and Cs) family of materials, which exhibit a complex relationship between the CDW and superconductivity, attracting substantial theoretical and experimental attention.[28–37] Specifically, extensive theoretical and experimental research on materials in the 135 family has yielded high-throughput first-principles calculations of other kagome candidates, including those with an AV_3Sb_5 prototype structure.[38,39] In addition to AV_3Sb_5, related V–Sb-based kagome metals, such as CsV_6Sb_6 and CsV_8Sb_{12}, have been synthesized and characterized,[40] providing additional platforms for exploring kagome-derived electronic states. Earlier studies on RMn_6X_6 (R = rare earth; X = Sn, Ge) materials, which possess a Mn-based kagome lattice and crystallize in the $HfFe_6Ge_6$-type structure ($P6/mmm$), have demonstrated complex magnetic orderings[41–51] and novel magneto-transport properties, including the anomalous Hall effect[52–59] and topological Hall effect.[55,56,60–68] Recently, the "166" materials exhibit behaviors akin to the "135" family, particularly with respect to electronic-order

†These authors contributed equally to this work.
*Corresponding author. Email: wangbt@ihep.ac.cn
© 2026 Chinese Physical Society and IOP Publishing Ltd. All rights, including for text and data mining, AI training, and similar technologies, are reserved.

phenomena tied to the kagome lattice. Nonmagnetic V ions have been substituted by Mn ions in the kagome layers, providing a clearer platform for studying the interplay between magnetism and the electronic structure derived from the kagome lattice. ScV_6Sn_6 exhibits a CDW transition at 92 K,[68–87] suggesting that charge order is a common feature of the partially filled d orbitals in this system. YV_6Sn_6, (Gd–Tm)V_6Sn_6, YbV_6Sn_6, and LuV_6Sn_6 have been studied using angle-resolved photoemission spectroscopy, revealing the presence of Dirac points, saddle points, and flat bands, which are indicative of nontrivial topological phases.[61–67,88–91] Moreover, recent angle-resolved photoemission spectroscopy measurements combined with first-principles calculations on RV_6Sn_6 (R = Gd, Tb, and Lu) demonstrated that the bands calculated without renormalization reproduced the main dispersive features, suggesting a weak electronic correlation in this vanadium-kagome family.[92]

One of the most compelling features of the "166" kagome compounds is their remarkable chemical versatility, allowing for the precise modulation of magnetic, topological, CDW, and/or superconducting states while maintaining independence from the kagome lattice. This flexibility provides a unique opportunity to investigate the complex interactions between these quantum states and the electronic structures derived from the kagome lattice. Compared with magnetic "166" kagome compounds, nonmagnetic kagome metals remain relatively underexplored. Theoretical predictions, particularly those guided by computational models, have proven to be invaluable for accelerating the discovery of new materials. Recent work by Ortiz *et al.* systematically examined the AM_6X_6 kagome metals and introduced the $LnNb_6Sn_6$ series, which demonstrate (1/3, 1/3, 1/3) CDW ordering as well as showcase the structural diversity and electronic flexibility of the "166" family, especially in nonmagnetic compounds.[93] Recently, Yang *et al.* reported Fermi-surface-driven frustration in the charge ordering of $LuNb_6Sn_6$. They observed pronounced softening of the flat optical phonon mode and competing charge-order correlations, highlighting strong coupling among Fermi-surface topology, phonons, and charge ordering in 166-type kagome metals.[94] Their findings provide compelling evidence that nonmagnetic kagome metals are thermodynamically and dynamically viable as well as have a rich potential for unconventional electronic behavior. These insights have significantly strengthened our confidence in systematically exploring the nonmagnetic domain of "166" kagome materials, aiming to uncover novel electronic states and possible superconductivity. In this study, we perform high-throughput first-principles screening of bilayer kagome AM_6X_6 compounds with the $MgFe_6Ge_6$-type ("166"-type) structure. For elements with f electrons, we adopt a consistent f-in-core treatment at the screening stage, and the quantitative electron–phonon coupling (EPC) discussions in this study were restricted to compounds without partially filled f shells. Among the 168 candidates, 157 compounds are found to be thermodynamically stable, 94 are dynamically stable, and 97 are nonmagnetic with zero total magnetic moment. By requiring simultaneous thermodynamic and dynamic stability, we identify 31 nonmagnetic metallic compounds as robust candidates for subsequent electronic structure and EPC analyses. Overall, our study provides a systematic stability map and EPC-based superconductivity assessment for the bilayer "166"-type kagome family, offering a practical theoretical database to guide future experimental synthesis and characterization.

Computation Methods. Our theoretical calculations were performed at the density functional theory (DFT)[95] level in high-throughput mode to screen for potential superconducting bilayer kagome materials. Crystal structure optimization and electronic structure calculations were performed using the QUANTUM ESPRESSO package. Ultrasoft pseudopotentials[96] were employed to model electron–ion interactions, while exchange-correlation effects were treated within the generalized gradient approximation using Perdew–Burke–Ernzerhof (PBE) functionals.[97] Van der Waals interactions were considered using Grimme's DFT-D3 correction, as implemented in structural relaxation.[98] The default PBE-associated parameter set (zero damping) was adopted in this implementation. This method was validated as effective in describing the isostructural kagome family of materials.[20] To ensure convergence, the cutoff energies were set to 80 Ry for the wave functions and 800 Ry for the charge density. The Gaussian smearing method with a smearing parameter of $\sigma = 0.01$ Ry was applied to calculate the charge density. The Brillouin zone (BZ) was sampled using a $16\times16\times12$ k-point mesh for structural optimization. All structures were fully relaxed until the force acting on each atom was less than 10^{-5} Ry/Å and the total energy convergence threshold was set as 10^{-6} Ry. Plane-wave cutoffs and BZ samplings were validated using convergence tests on representative compounds. The chosen parameters ensure that the total energy, phonon frequencies, and EPC-related quantities converge within a practically negligible numerical uncertainty for high-throughput screening.

The phonon dispersion curves were obtained using the density functional perturbation theory,[99] where a denser $20\times20\times12$ k-point grid and a $5\times5\times3$ q-point grid were employed for the EPC calculations. The superconducting critical temperature T_c was calculated based on the Allen–Dynes-modified McMillan formula:[100]

$$T_c = \frac{\omega_{\log}}{1.2}\exp\left[-\frac{1.04(1+\lambda)}{\lambda-\mu^*-0.62\lambda\mu^*}\right], \tag{1}$$

where μ^* is the effective Coulomb pseudopotential and the integrated EPC constant can be obtained as follows:

$$\lambda(\omega) = 2\int_0^{\omega}\frac{\alpha^2F(\omega)}{\omega}\mathrm{d}\omega. \tag{2}$$

Here, $\omega_{\log}$ is the logarithmically averaged characteristic phonon frequency, which is defined as

$$\omega_{\log} = \exp\left[\frac{2}{\lambda}\int\frac{\mathrm{d}\omega}{\omega}\alpha^2F(\omega)\ln\omega\right]. \tag{3}$$

Spin–orbit coupling (SOC) was excluded in the high-throughput screening because of the substantial computational cost associated with large-scale phonon and EPC

calculations. The present study aims to capture the qualitative trends of weak-coupling superconductivity within the Allen–Dynes framework. Rare-earth elements were treated using f-in-core pseudopotentials, in which 4f electrons were included in the frozen core. Accordingly, the quantitative superconducting properties in this study are discussed only for compounds without partially filled f shells, whereas rare-earth-containing systems are included mainly to illustrate the qualitative chemical and structural trends. Furthermore, the transition-metal d states in the considered nonmagnetic metallic AM_6X_6 compounds are relatively itinerant and form broad bands around the Fermi level. Therefore, within the scope of our high-throughput screening (thermodynamic/dynamical stability and weak-coupling EPC trends), introducing an on-site Hubbard U is not expected to qualitatively change the stability criteria, phonon spectra, or the overall ranking of EPC-derived T_c. DFT+U was excluded in the workflow for consistency and computational efficiency across a large material space. This is consistent with recent studies on RV_6Sn_6 (R = Gd, Tb, and Lu), where the main band dispersions were reproduced without renormalization, suggesting a weak electronic correlation in this V-kagome family.[92]

Results and Discussion.

Crystal Structures and Stability. In this study, 168 AM_6X_6 compounds with $HfFe_6Ge_6$-type structure ($P6/mmm$) were systematically investigated using a high-throughput computational workflow. The parent structure belongs to the hexagonal space group (No. 191), as verified by single-crystal X-ray diffraction data.[61] This layered kagome-based parent structure has been previously observed in both magnetic and nonmagnetic compounds, such as RMn_6X_6 (R = rare earth, X = Sn/Ge) and ScV_6Sn_6,[38,93] exhibiting diverse magnetic and electronic behaviors depending on the elemental filling. The "A" element is drawn from the group of elements highlighted in indigo in Fig. 1(a), which includes hydrogen, alkali metals, alkaline metals and rare-earth metals. The "M" element is selected from the orange highlighted group, comprising the transition metals V, Nb, and Ta. The "X" element stands for Sb and Sn, highlighted by the green set. Compared with the AV_3Sb_5 "135" kagome family, which features a single kagome layer with minimal interlayer interaction,[31] the AM_6X_6 structure incorporates two kagome layers separated by triangular ($AX2$) and honeycomb ($X1X3$) sublattices, forming a bilayer kagome motif with enhanced geometric complexity. As illustrated in Fig. 1(b), the unit cell comprises four distinct layers stacked along the c-axis: $X1$, $X2$, transition metal M, and $AX3$. The structural organization along the stacking direction defines the overall three-dimensional arrangement. The top view in Fig. 1(c) highlights the intricate atomic arrangements in the ab plane, where M atoms form the kagome network via corner-sharing triangles, A and $X2$ atoms construct triangular planes, and $X1/X3$ atoms assemble into a honeycomb-like structure that interlinks the double kagome layers. The A–A segment shown in Fig. 1(c) indicates the nearest-neighbor A-site separation within the triangular layer and should not be interpreted as a direct covalent bond. Although the geometric $X3$–$X3$ distances are comparable, the $X3$ atoms mainly bond with neighboring M/X atoms within the framework and do not form a direct $X3$–$X3$ bond. This structural configuration is consistent with the $MgFe_6Ge_6$-type kagome metals recently investigated by high-throughput DFT screening,[38]

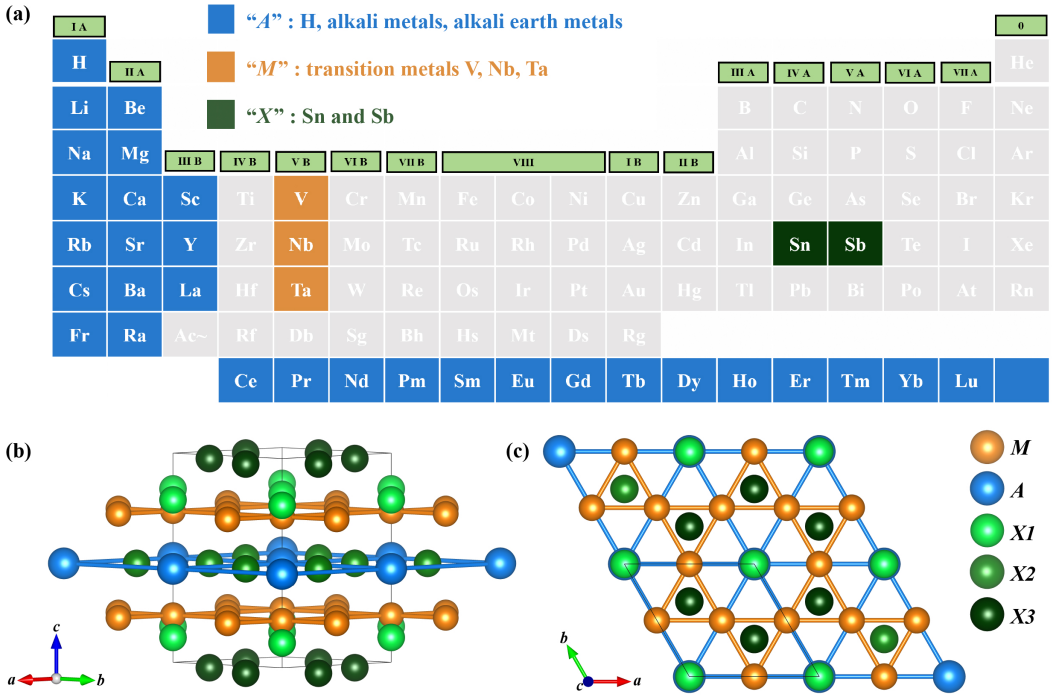

Fig. 1. (a) Selected elements in building of an AM_6X_6 material. The blue, orange, and dark green squares represents A, M, and X atoms, respectively. (b) and (c) are the crystal structures of the AM_6X_6 structure along the z-direction and parallel to the z-direction, respectively. In panel (c), the lines connecting the A sites are drawn only to indicate the nearest-neighbor A–A separation within the triangular layer and should not be interpreted as covalent bonds.

where the flexibility of atomic stacking permits diverse modulations of symmetry, bonding, and dimensionality. Notably, while both the "135" and "166" structures share identical hexagonal lattice symmetry ($P6/mmm$), the unit cell of AM_6X_6 displays more sophisticated layering and variable coordination environments, which are expected to influence their electronic instabilities, such as CDW formation,[68–81,83–87,93] orbital hybridization, or even superconductivity. These structural distinctions open new avenues for exploring novel quantum states in kagome-lattice-based materials.

The synthesizability of a compound is predominantly dictated by its thermodynamic stability and the dynamic factors governing its growth. Therefore, a compound must thermodynamically compete with all possible phases within the same chemical composition space, ultimately stabilizing the most energetically favorable phase. Consequently, assessing the likelihood of a compound's existence becomes more feasible if the formation energies of all stable and competing phases are determined. The formation energy of a compound, often referred to as the standard enthalpy of formation, quantifies the enthalpy change associated with the formation of a compound from its constituent pure elements under identical conditions.[101] A negative formation energy indicates an exothermic process, signifying the release of energy and relative thermodynamic stability of the compound. Conversely, a positive formation energy denotes an endothermic process and implies that the compound is less stable than its elemental constituents. To evaluate the thermodynamic stability of the AM_6X_6 system, we calculated the formation energy (E_f) as follows:

$$E_\mathrm{f} = \frac{E_{AM_6X_6} - E_A - 6E_M - 6E_X}{13}.$$

All calculations were performed using consistent parameters and the elemental structures sourced from the Materials Project database[102] to ensure reliable reference energies and phase diagram construction. The results of thermodynamic calculations are shown in Fig. 2(a). The white boxes highlight structures with positive E_f values that are thermodynamically unstable, indicating that these compounds are energetically unfavorable. The dark green represent structures with higher thermodynamic stabilities, whereas the green boxes correspond to those with lower stabilities. Notably, the formation energy alone may not always provide a complete picture of synthesizability. Some metastable materials (e.g., those with a slightly positive E_f) can be realized experimentally under nonequilibrium or high-pressure conditions.[103]

Among the 157 thermodynamically stable structures, clear chemical trends were observed for the A- and X-site elements. Generally, replacing alkali-metal A-site cations with alkaline-earth cations lowers the formation energy,

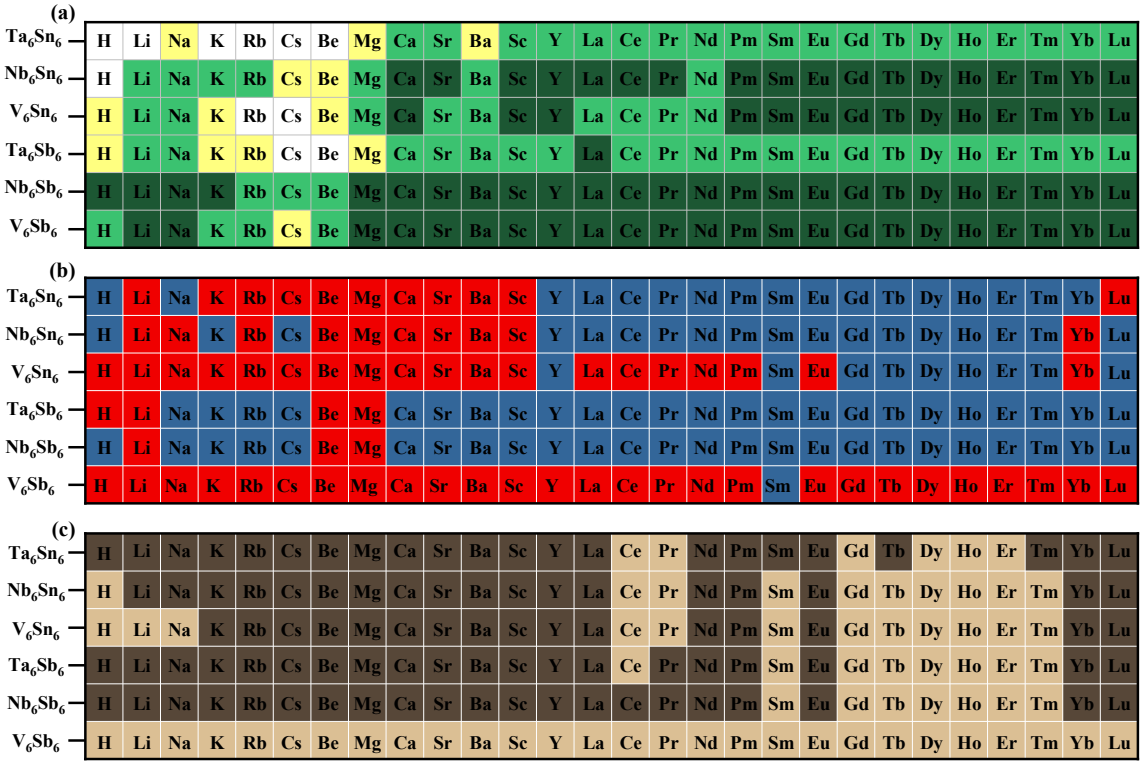

Fig. 2. High-throughput screening of stability and magnetic properties of AM_6X_6 compounds. (a) Formation energies of AM_6X_6 compounds relative to competing phases, shown as thermodynamic stability regions for high-throughput screening rather than quantitative energetic ranking. Dark green, green, and yellow correspond to the formation-energy ranges of $\Delta E < -30$ meV/atom, $-30 \le \Delta E < -10$ meV/atom, and $\Delta E \ge -10$ meV/atom, respectively. (b) Dynamical stability map obtained from DFPT phonon calculations. The blue squares indicate dynamically stable compounds without imaginary phonon modes, while the red squares correspond to dynamically unstable cases. (c) Magnetic screening results. The dark-colored squares represent nonmagnetic solutions (zero magnetic moment), while the light-colored squares indicate magnetic ground states.

indicating improved thermodynamic stability within the AM_6X_6 framework. In addition, Sb-based compounds typically exhibit lower formation energies than their Sn-based analogs. These stability trends are consistent with previous high-throughput screening of related kagome candidates (e.g., Cai *et al.*[38]). Physically, the enhanced stability can be understood mainly in terms of ionic-size compatibility, electrostatic interactions, and favorable structural matching between the A-site cations and the bilayer kagome framework, rather than simplistic arguments based on electronegativity or ionization tendencies. Rare-earth-containing compositions were included in our dataset to illustrate broad chemical trends. However, as discussed in the Computational Methods section, the lattice dynamic properties of partially filled f-shell systems are sensitive to the treatment of f electrons. Therefore, although qualitative chemical stability trends remain meaningful, quantitative discussions of the lattice dynamics, EPC, and superconducting properties of these systems are beyond the scope of this study.

To evaluate the dynamic stabilities of all the proposed compounds, we calculated their phonon dispersions. The absence of imaginary frequencies in the phonon modes demonstrates dynamical stability. Figure 2(b) summarizes the critical properties of the phonon dispersions of all 168 AM_6X_6 compounds, where the red squares correspond to compounds exhibiting imaginary phonon frequencies, indicating dynamic instability, whereas the blue squares represent those with real phonon frequencies, signifying dynamic stability. Our results indicate that a total number of 94 "166" bilayer kagome compounds are dynamically stable. This number is significantly smaller than that of the thermodynamically stable compounds, highlighting the complex relationship between the two stability criteria. In general, materials containing the V_6Sb_6 motif are dynamically unstable, with the exception of SmV_6Sb_6. However, most structures containing Nb_6Sb_6 are dynamically stable, except $LiNb_6Sb_6$, $BeNb_6Sb_6$, and $MgNb_6Sb_6$. A similar trend is observed for materials containing Ta_6Sb_6, with the majority being dynamically stable, except HTa_6Sb_6, $LiTa_6Sb_6$, $BeTa_6Sb_6$, and $MgTa_6Sb_6$.

For materials incorporating Sn, we can observe that most alkali- and alkaline-earth-based structures are dynamically unstable, except HNb_6Sn_6, KNb_6Sn_6, $CsNb_6Sn_6$, HTa_6Sn_6, and $NaTa_6Sn_6$. Overall, Nb- and Ta-based kagome layers tend to yield improved dynamic stability compared to V-based kagome layers, which is consistent with the trend already observed for Sb-based compounds. Several rare-earth V_6Sn_6 members known experimentally (e.g., YV_6Sn_6,[61,65,88] (Gd–Tm)V_6Sn_6,[61,63–65,89,90] YbV_6Sn_6, and LuV_6Sn_6[65]) were predicted to be dynamically stable in our screening, supporting the reliability of the present DFPT workflow at the qualitative level. However, as discussed in the Computational Methods section, the lattice-dynamical properties of partially filled f-shell systems can be sensitive to the treatment of f electrons. Therefore, the rare-earth-containing results in the present work are typically used to illustrate qualitative chemical and structural trends, whereas quantitative discussions of phonon spectra, EPC, and superconducting properties are restricted to compounds without partially filled f shells.

Our research focuses on identifying stable structures without magnetism within the "166" family. Therefore, we performed magnetic moment calculations for each material to assess the presence of magnetic order. The magnetic moments of these materials were calculated using the spin-polarization method in DFT,[104] which considers complex spin interactions and non-collinear magnetic configurations. The results of these calculations are shown in Fig. 2(c). The dark brown regions represent materials with zero magnetic moments, whereas the light brown regions indicate materials with non-zero magnetic moments, signifying the presence of magnetism. Evidently, materials containing V_6Sn_6, as well as those with Gd-, Dy-, Ho-, and Er-based motifs, exhibit non-zero magnetic moments, indicating that these materials possess intrinsic magnetic properties. However, among all the structures considered, 97 materials were found to have zero magnetic moments, indicating that they were nonmagnetic materials. This distinction is crucial for the subsequent analyses of superconductivity.

Phonon Vibrations and Superconductivity. To fully understand the phonon vibration properties, we calculated the phonon dispersion curves of all compounds [Figs.S2–S19 in the Supplementary Material (SM)]. The phonon spectra of KV_6Sb_6, KTa_6Sn_6, $CsTa_6Sn_6$, GdV_6Sb_6, DyV_6Sb_6, HoV_6Sb_6, ScV_6Sn_6, LaV_6Sn_6, and CeV_6Sn_6 show that the phonon frequencies on the path from high-symmetry points A to L tend to zero or even become imaginary, indicating that the phonon modes are unstable on this wave vector, to reduce the energy through lattice distortion along the phonon eigenvector. This instability may be related to the CDW phase transition.[105–108] Notably, the CDW transition of ScV_6Sn_6 has been experimentally confirmed and widely discussed,[68–87] further supporting the reliability of the present phonon calculations.

We further evaluated the superconducting properties of structures that are thermodynamically and dynamically stable, nonmagnetic, and metallic. The calculated EPC constant λ, logarithmic average phonon frequency $\omega_{\log}$, and superconducting transition temperature T_c are summarized in Table S1 of the SM. Consistent with the scope defined in the Computational Methods section, Table S1 in SM includes only compounds without partially filled f shells for which the present framework provides a reliable quantitative description. To evaluate the sensitivity to the Coulomb pseudopotential, T_c values are provided for both $\mu^* = 0.10$ and $\mu^* = 0.13$. The resulting λ values range from 0.37 to 0.62, and T_cs are positively correlated with the amplitudes of λ, ranging from 0.650 to 3.968 K. Figure 3 shows the distribution of T_cs, with red representing a higher T_cs and purple representing a lower T_cs. The T_cs values of materials with the same M_6X_6 units are similar. In general, the materials containing Sb exhibit higher T_cs than those containing Sn atoms. The A atom appears to have a limited effect on T_c. Among the transition metal atoms V, Nb, and Ta, which form kagome layers, materials containing Nb atoms show larger values of T_c. In the following, we focus on four representative compounds,

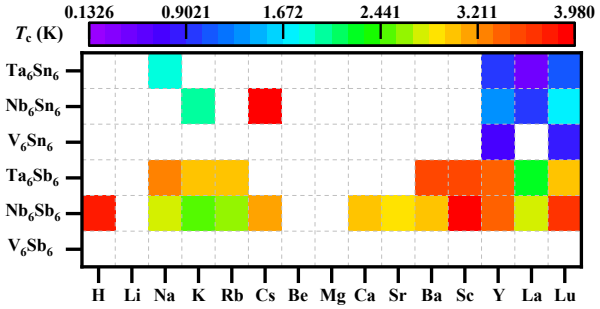

Fig. 3. Calculated superconducting transition temperatures T_c of nonmagnetic AM_6X_6 compounds obtained from electron–phonon coupling calculations within the Allen–Dynes formalism. Only compounds without partially filled f shells are included, for which the present theoretical framework is expected to provide a meaningful description of weak-coupling superconductivity. The blank regions indicate compositions that are not considered in the quantitative T_c analysis.

HNb_6Sb_6, $ScNb_6Sb_6$, $LuNb_6Sb_6$, and $CsNb_6Sn_6$, which exhibit the highest superconducting transition temperatures among dynamically stable materials. These systems were selected to elucidate the lattice-dynamical and EPC characteristics of the bilayer kagome family. Table S2 in SM summarizes the optimized lattice parameters and atomic fractional coordinates of these compounds, demonstrating their reproducibility. The phonon spectra and vibrational characteristics are presented in Fig. 4. For HNb_6Sb_6, the vibrations of H atoms are concentrated in the high-frequency region (100–700 cm^{-1}), with a clear separation between the in-plane and out-of-plane vibrations. The Nb atomic vibrations mainly distribute intermediate-frequency region of 100–200 cm^{-1}, where the in-plane and out-of-plane vibrations are coupled. The Sb atomic vibrations are typically in the low-frequency range of 0–200 cm^{-1}, with the soft modes typically emerging from the out-of-plane (z-direction) vibrations. The phonon vibration modes of $ScNb_6Sb_6$ and $LuNb_6Sb_6$ are similar, although the out-of-plane vibrations of the Lu atoms are nearly negligible. In these systems, Nb atoms vibrate in the mid- to high-frequency regions, whereas Sb atoms vibrate in the mid- to low-frequency regions. In $CsNb_6Sn_6$, the in-plane and out-of-plane vibrations of the Cs atoms exhibit partial coupling. The out-of-plane vibrations of Nb atoms dominate the high-frequency region (175–225 cm^{-1}), whereas in-plane vibrations are primarily distributed in the mid-frequency range (120–230 cm^{-1}). Notably, the acoustic soft mode typically originates from the z-direction vibrations of Sn atoms. Normally, soft modes are beneficial for enhancing the EPC and superconductivity.[100,109,110] Detailed phonon vibration data for all selected superconducting materials are provided in SM, serving as a valuable reference for future theoretical and experimental studies.

The phonon dispersions weighted by the magnitude of the phonon linewidth γ_{qv}, Eliashberg electron–phonon spectral function $\alpha^2F(\omega)$, and cumulative frequency dependence of the EPC constant λ are illustrated in Fig. 5. The phonon linewidth can be estimated as

$$\gamma_{qv} = 2\pi\omega_{qv}\sum_{ij}\int\frac{\mathrm{d}^3k}{\Omega_{\mathrm{BZ}}}|g_{qv}(k,i,j)^2| \times \delta(\varepsilon_{q,i}-\varepsilon_{\mathrm{F}})\delta(\varepsilon_{k+q,j}-\varepsilon_{\mathrm{F}}),$$

where Ω_{BZ} is the volume of the BZ, $\varepsilon_{q,i}$ and $\varepsilon_{k+q,j}$ denote the Kohn–Sham energies, and $g_{q,v}(k,i,j)$ represents the EPC matrix element.[100] $g_{q,v}(k,i,j)$, which can be determined self-consistently using the linear response theory, describes the probability amplitude for electron scattering accompanied by the transfer of crystal momentum q.[100]

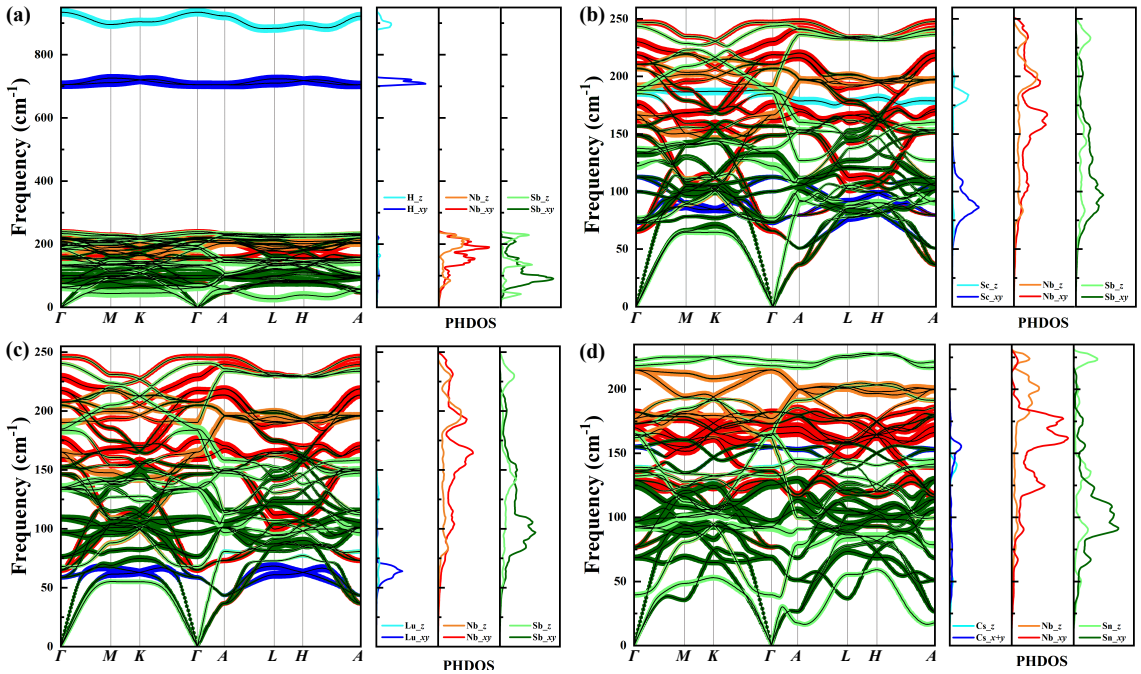

Fig. 4. Phonon dispersions weighted by different atomic vibrational modes and vibrational mode resolved (colored lines) phonon density of states of (a) HNb_6Sb_6, (b) $ScNb_6Sb_6$, (c) $LuNb_6Sb_6$, and (d) $CsNb_6Sn_6$.

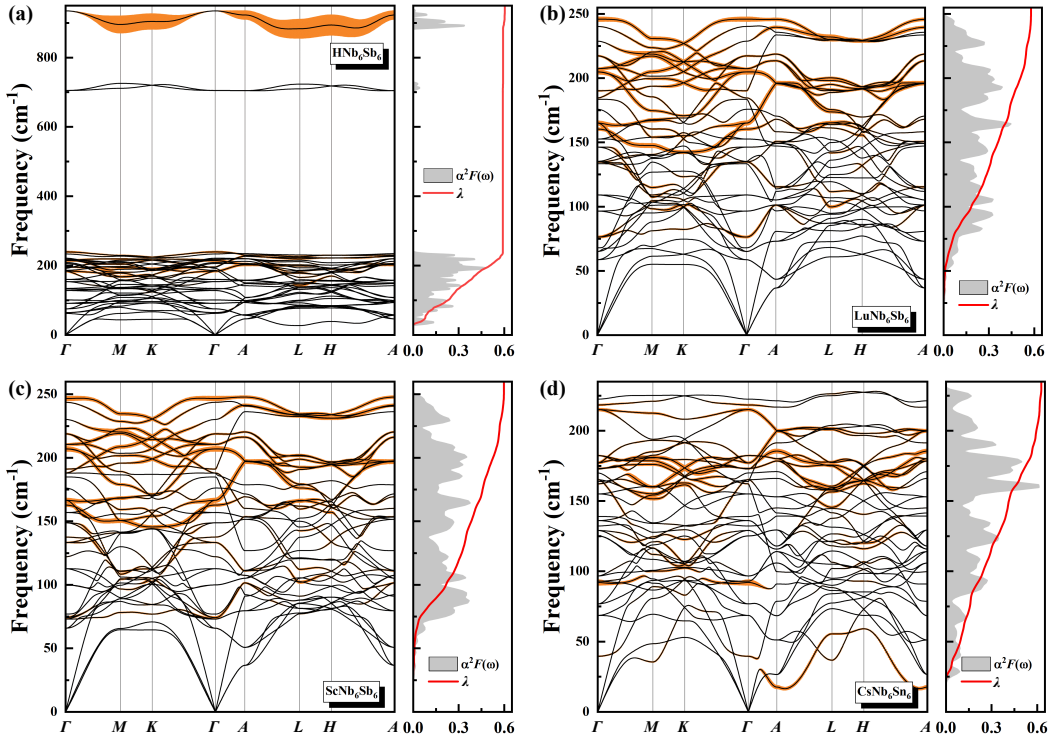

Fig. 5. (a) Phonon dispersions weighted by the magnitude of the phonon linewidth (orange circles) for HNb_6Sb_6. The right panel indicates the Eliashberg spectral function $\alpha^2F(\omega)$ (gray shading) and integrated strength of EPC of $\lambda(\omega)$ (red line). (b), (c), and (d) are the same as (a) but for $ScNb_6Sb_6$, $LuNb_6Sb_6$, and $CsNb_6Sn_6$, respectively.

Note that γ_{qv} reflects the EPC contribution, which does not depend on the real or imaginary character of the phonon frequency.[111] Figure 5(a) shows that the main contribution to the phonon linewidth (and consequently to the EPC) in HNb_6Sb_6 comes from the out-of-plane (in the z direction) vibration of H atoms, with a small contribution from the Nb atoms. For both $ScNb_6Sb_6$ and $LuNb_6Sb_6$, the main contribution to the phonon linewidth was from the vibrations of the Nb atoms. For $CsNb_6Sn_6$, the contribution to the phonon linewidth originates from both the vibration of the kagome layer and the z-direction vibration of the Sn atoms, particularly the soft mode in the low-frequency region. This behavior is consistent with that of $LuNb_6Sn_6$, where a flat optical phonon branch exhibits pronounced softening and is closely associated with the CDW formation in the 166-type kagome metal.[94]

Overall, across all the materials investigated, the A-site atoms exhibited a broad range of vibrational distributions owing to the differences in atomic mass. However, except for HNb_6Sb_6, the contribution of the A-site vibrations to the superconducting properties was negligible. Instead, the primary contribution to the phonon linewidth, and thus to the EPC, originates mainly from the vibrations of the kagome layer formed by the transition metal atoms. Furthermore, our analysis revealed that the choice of transition metal (M) has a profound impact on T_c. Specifically, when M was Nb, the T_cs values were significantly higher than those of V or Ta. This highlighted the critical role of Nb in enhancing the superconductivity of these materials. An intriguing observation was made for materials containing Sn atoms, which consistently displayed pronounced soft phonon modes in the low-frequency region. These soft modes are typically associated with the out-of-plane vibrations of Sn atoms along the z-direction. This unique vibrational behavior of the Sn atoms makes a notable contribution to the superconducting properties of the material, underscoring the role of specific atomic dynamics in tailoring superconductivity. Considering that conventional "166" systems typically exhibit robust magnetic ordering,[10,41,112–114] we focus on identifying a stable AM_6X_6 structure that deviates from this norm by being nonmagnetic. This unique configuration, which we identify as a weak superconductor, overcomes the conventional rule. Our findings present a valuable opportunity to explore novel properties and phenomena within the "166" kagome systems.

Recent theoretical investigations have begun to explore the nonmagnetic variants of kagome-layered materials within the "166" structure type. For example, Yi *et al.*[36] conducted first-principles calculations focusing on a limited set of AM_6X_6 materials and predicted several nonmagnetic compounds with potential superconductivity; however, they did not perform detailed phonon calculations or evaluate the EPC strength. Similarly, Cai *et al.*[35] applied high-throughput methods to a broader set of kagome candidates but typically focused on the identification of topological phases and CDW-related instabilities without systematically addressing superconductivity or EPC.

In contrast, this work presents a comprehensive high-throughput screening that combines thermodynamic, dynamic, and magnetic stability assessments with full

phonon and EPC analysis for 168 AM_6X_6 compounds. Notably, we identified 59 stable nonmagnetic metallic materials and determined their superconducting transition temperatures (T_cs), EPC constants, and phonon linewidth-resolved contributions. This represents the first systematic effort to map out the weak-coupling BCS superconductivity landscape in the bilayer kagome AM_6X_6 family. By integrating the lattice dynamics and electronic structure analyses, our results bridge a critical gap in the theoretical study of kagome superconductors and offer guidance for experimental synthesis and verification.

Conclusions. The stability and superconducting properties of the bilayer kagome AM_6X_6 family were systematically investigated using high-throughput first-principles calculations within the Allen–Dynes framework. A comprehensive analysis of 168 compounds was performed to evaluate their thermodynamic and dynamic stability, as well as magnetic moments, using a consistent set of computational parameters. We identified 157 thermodynamically stable materials, 94 dynamically stable materials, and 97 materials exhibiting zero magnetic moments. Thermodynamic stability is strongly influenced by the A-site chemistry (alkali vs. alkaline earth) and the X-site element, with Sb-based compounds generally exhibiting lower formation energies than Sn-based compounds. Phonon calculations revealed that Nb- and Ta-based kagome layers are generally more dynamically stable than V-based layers, with several materials exhibiting soft modes, indicative of proximity to CDW-like lattice instabilities. Focusing on compounds without partially filled f shells, we found weak-coupling BCS superconductivity with T_c ranging from 0.65 to 3.97 K. The dominant contribution to EPC originates from kagome-layer vibrations, with Sn atoms introducing low-frequency out-of-plane soft modes that further enhance lambda. Overall, this study provides a practical database and guiding principles for the design and experimental exploration of bilayer kagome superconductors in the AM_6X_6 family.

Acknowledgments. B.-T.W. gratefully acknowledges financial support from the Guangdong Provincial Quantum Science Strategic Initiative (Grant No. GDZX2501011), the Guangdong Basic and Applied Basic Research Foundation (Grant No. 2024A1515010484), and the National Natural Science Foundation of China (Grant Nos. U2330104 and 12574028). P.Z. gratefully acknowledges the financial support from the National Key R&D Program of China (Grant No. 2022YFA1403103). L.-T.S. gratefully acknowledges the financial support from the Guangdong Basic and Applied Basic Research Foundation (Grant No. 2022A1515110404). J.-G.S. acknowledges financial support from the National Natural Science Foundation of China (Grant No. 12304095), the Guangdong Basic and Applied Basic Research Foundation (Grant No. 2023A1515140188), and the China Postdoctoral Science Foundation (Grant No. 2024M762275). H.-B.Z. acknowledges support from the National Natural Science Foundation of China (Grant No. 12404190) and the Guangdong Basic and Applied Basic Research Foundation (Grant No. 2022A1515110322). The calculations were performed using the CSNS Scientific Computing Platform of the Institute of High Energy Physics of CAS and the GBA Subcenter of the National HEP Science Data Center.

References

[1] Syôzi I 1951 *Prog. Theor. Phys.* **6** 306
[2] Ohgushi K, Murakami S, and Nagaosa N 2000 *Phys. Rev. B* **62** R6065
[3] Mazin I, Jeschke H O, Lechermann F, Lee H, Fink M, Thomale R, and Valenti R 2014 *Nat. Commun.* **5** 4261
[4] Ye L, Kang M, Liu J, von Cube F, Wicker C R, Suzuki T, Jozwiak C, Bostwick A, Rotenberg E, Bell D C, Fu L, Comin R, and Checkelsky J G 2018 *Nature* **555** 638
[5] Liu Z, Liu F, and Wu Y S 2014 *Chin. Phys. B* **23** 077308
[6] Kang M, Ye L, Fang S, You J S, Levitan A, Han M, Facio J I, Jozwiak C, Bostwick A, Rotenberg E, Chan M K, McDonald R D, Graf D, Kaznatcheev K, Vescovo E, Bell D C, Kaxiras E, van den Brink J, Richter M, Prasad Ghimire M, Checkelsky J G, and Comin R 2020 *Nat. Mater.* **19** 163
[7] Beugeling W, Everts J C, and Morais Smith C 2012 *Phys. Rev. B* **86** 195129
[8] Guo H M and Franz M 2009 *Phys. Rev. B* **80** 113102
[9] Yin J X, Zhang S S, Chang G, Wang Q, Tsirkin S S, Guguchia Z, Lian B, Zhou H, Jiang K, Belopolski I, Shumiya N, Multer D, Litskevich M, Cochran T A, Lin H, Wang Z, Neupert T, Jia S, Lei H, and Hasan M Z 2019 *Nat. Phys.* **15** 443
[10] Ghimire N J, Dally R L, Poudel L, Jones D C, Michel D, Magar N T, Bleuel M, McGuire M A, Jiang J S, Mitchell J F, Lynn J W, and Mazin I I 2020 *Sci. Adv.* **6** eabe2680
[11] Kang M, Fang S, Ye L, Po H C, Denlinger J, Jozwiak C, Bostwick A, Rotenberg E, Kaxiras E, Checkelsky J G, and Comin R 2020 *Nat. Commun.* **11** 4004
[12] Kida T, Fenner L A, Dee A A, Terasaki I, Hagiwara M, and Wills A S 2011 *J. Phys.: Condens. Matter* **23** 112205
[13] Liu E, Sun Y, Kumar N, Muchler L, Sun A, Jiao L, Yang S Y, Liu D, Liang A, Xu Q, Kroder J, Suss V, Borrmann H, Shekhar C, Wang Z, Xi C, Wang W, Schnelle W, Wirth S, Chen Y, Goennenwein S T B, and Felser C 2018 *Nat. Phys.* **14** 1125
[14] Wang Q, Xu Y, Lou R, Liu Z, Li M, Huang Y, Shen D, Weng H, Wang S, and Lei H 2018 *Nat. Commun.* **9** 1
[15] Zhou H, Liu H, Ji H, Li X, Meng S, and Sun J T 2023 *npj Quantum Mater.* **8** 16
[16] Chen D, Le C, Fu C, Lin H, Schnelle W, Sun Y, and Felser C 2021 *Phys. Rev. B* **103** 14441
[17] Chen K Y, Wang N N, Yin Q W, Gu Y H, Jiang K, Tu Z J, Gong C S, Uwatoko Y, Sun J P, Lei H C, Hu J P, and Cheng J G 2021 *Phys. Rev. Lett.* **126** 247001
[18] Zhao Y, Nie Z, Hong H, Qiu X, Han S, Yu Y, Liu M, Qiu X, Liu K, Meng S, Tong L, and Zhang J 2023 *Nat. Commun.* **14** 2223
[19] Teng X, Chen L, Ye F, Rosenberg E, Liu Z, Yin J X, Jiang Y X, Oh J S, Hasan M Z, Neubauer K J, Gao B, Xie Y, Hashimoto M, Lu D, Jozwiak C, Bostwick A, Rotenberg E, Birgeneau R J, Chu J H, Yi M, and Dai P 2022 *Nature* **609** 490
[20] Tan H, Liu Y, Wang Z, and Yan B 2021 *Phys. Rev. Lett.* **127** 046401
[21] Guguchia Z, Mielke C, Das D, Gupta R, Yin J X, Liu H, Yin Q, Christensen M H, Tu Z, Gong C, Shumiya N, Hossain M S, Gamsakhurdashvili T, Elender M, Dai P, Amato A, Shi Y, Lei H C, Fernandes R M, Hasan M Z, Luetkens H, and Khasanov R 2023 *Nat. Commun.* **14** 153
[22] Yu S L and Li J X 2012 *Phys. Rev. B* **85** 144402

[23] Jiang Y X, Yin J X, Denner M M, Shumiya N, Ortiz B R, Xu G, Guguchia Z, He J, Hossain M S, Liu X, Ruff J, Kautzsch L, Zhang S S, Chang G, Belopolski I, Zhang Q, Cochran T A, Multer D, Litskevich M, Cheng Z J, Yang X P, Wang Z, Thomale R, Neupert T, Wilson S D, and Hasan M Z 2021 *Nat. Mater.* **20** 1353

[24] Li H, Cheng S, Ortiz B R, Tan H, Werhahn D, Zeng K, Johrendt D, Yan B, Wang Z, Wilson S D, and Zeljkovic I 2023 *Nat. Phys.* **19** 1591

[25] Nie L, Sun K, Ma W, Song D, Zheng L, Liang Z, Wu P, Yu F, Li J, Shan M, Zhao D, Li S, Kang B, Wu Z, Zhou Y, Liu K, Xiang Z, Ying J, Wang Z, Wu T, and Chen X 2022 *Nature* **604** 59

[26] Liang Z, Hou X, Zhang F, Ma W, Wu P, Zhang Z, Yu F, Ying J J, Jiang K, Shan L, Wang Z, and Chen X H 2021 *Phys. Rev. X* **11** 031026

[27] Ding P, Lee C H, Wu X, and Thomale R 2022 *Phys. Rev. B* **105** 174518

[28] Ortiz B R, Gomes L C, Morey J R, Winiarski M, Bordelon M, Mangum J S, Oswald I W H, Rodriguez-Rivera J A, Neilson J R, Wilson S D, Ertekin E, McQueen T M, and Toberer E S 2019 *Phys. Rev. Mater.* **3** 094407

[29] Ortiz B R, Sarte P M, Kenney E M, Graf M J, Teicher S M L, Seshadri R, and Wilson S D 2021 *Phys. Rev. Mater.* **5** 034801

[30] Yin Q, Tu Z, Gong C, Fu Y, Yan S, and Lei H 2021 *Chin. Phys. Lett.* **38** 037403

[31] Ortiz B R, Teicher S M L, Hu Y, Zuo J L, Sarte P M, Schueller E C, Abeykoon A M M, Krogstad M J, Rosenkranz S, Osborn R, Seshadri R, Balents L, He J, and Wilson S D 2020 *Phys. Rev. Lett.* **125** 247002

[32] Kang M, Fang S, Kim J K, Ortiz B R, Ryu S H, Kim J, Yoo J, Sangiovanni G, Di Sante D, Park B G, Jozwiak C, Bostwick A, Rotenberg E, Kaxiras E, Wilson S D, Park J H, and Comin R 2022 *Nat. Phys.* **18** 301

[33] Ortiz B R, Teicher S M L, Kautzsch L, Sarte P M, Ratcliff N, Harter J, Ruff J P C, Seshadri R, and Wilson S D 2021 *Phys. Rev. X* **11** 041030

[34] Hu Y, Wu X, Ortiz B R, Ju S, Han X, Ma J, Plumb N C, Radovic M, Thomale R, Wilson S D, Schnyder A P, and Shi M 2022 *Nat. Commun.* **13** 2220

[35] Ni S, Ma S, Zhang Y, Yuan J, Yang H, Lu Z, Wang N, Sun J, Zhao Z, Li D, Liu S, Zhang H, Chen H, Jin K, Cheng J, Yu L, Zhou F, Dong X, Hu J, Gao H J, and Zhao Z 2021 *Chin. Phys. Lett.* **38** 057403

[36] Mu C, Yin Q, Tu Z, Gong C, Lei H, Li Z, and Luo J 2021 *Chin. Phys. Lett.* **38** 077402

[37] Chen X, Zhan X, Wang X, Deng J, Liu X B, Chen X, Guo J G, and Chen X 2021 *Chin. Phys. Lett.* **38** 057402

[38] Cai G, Jiang Y, Zhou H, Yu Z, Jiang K, Shi Y, Meng S, and Liu M 2023 *Chin. Phys. Lett.* **40** 117101

[39] Yi X W, Ma X Y, Zhang Z, Liao Z W, You J Y, and Su G 2022 *Phys. Rev. B* **106** L220505

[40] Yin Q, Tu Z, Gong C, Tian S, and Lei H 2021 *Chin. Phys. Lett.* **38** 127401

[41] Venturini G, Idrissi B C E, and Malaman B 1991 *J. Magn. Magn. Mater.* **94** 35

[42] Amako Y, Yamamoto T, Misawa M, Yoshie H, and Nagai H 1995 *J. Magn. Magn. Mater.* **140-144** 1029

[43] Malaman B, Venturini G, Idrissi B C E, and Ressouche E 1997 *J. Alloy. Compd.* **252** 41

[44] Gorbunov D I, Kuz'min M D, Uhlířová K, Žáček M, Richter M, Skourski Y, and Andreev A V 2012 *J. Alloys Compd.* **519** 47

[45] Chen Z, Li M, Liu C, Ma Z, Han Y, Gao J, Wei W, Sheng Z, and Du H 2021 *Front. Phys.* **9** 685510

[46] Koyama M, Narumi Y, Yoshii S, Kindo K, Zhang L, Brück E, Buschow K H J, Boer F R D, Lefèvre C, and Venturini G 2006 *J. Alloys Compd.* **408-412** 161

[47] Kelemen M T, Rosch P, Dormann E, and Buschow K H J 2001 *J. Magn. Magn. Mater.* **223** 253

[48] Uhlířová K, de Boer F R, Sechovsky V, Yoshii S, Nakagawa Y, Hagiwara M, Kindo K, and Venturini G 2007 *J. Magn. Magn. Mater.* **316** e422

[49] Uhlířová, Sechovsky V, Boer F R d, Yoshii S, Nishikawa K, Hagiwara M, Kindo K, and Venturini G 2006 *J. Magn. Magn. Mater.* **51** 123

[50] Mar A, Lefèvre C, and Venturini G 2004 *J. Magn. Magn. Mater.* **269** 380

[51] Yoshii S, Kindo K, Zhang L, Brück E, Buschow K H J, de Boer F R, Lefèvre C, and Venturini G 2006 *J. Alloys Compd.* **408-412** 173

[52] Uhlířová K, Sechovsky V, de Boer F R, Yoshii S, Yamamoto T, Hagiwara M, Lefèvre C, and Venturini G 2007 *J. Magn. Magn. Mater.* **310** 1747

[53] Asaba T, Thomas S M, Curtis M, Thompson J D, Bauer E D, and Ronning F 2020 *Phys. Rev. B* **101** 174415

[54] Ma W, Xu X, Yin J X, Yang H, Zhou H, Cheng Z J, Huang Y, Qu Z, Wang F, Hasan M Z, and Jia S 2021 *Phys. Rev. Lett.* **126** 246602

[55] Dhakal G, Cheenicode Kabeer F, Pathak A K, Kabir F, Poudel N, Filippone R, Casey J, Pradhan Sakhya A, Regmi S, Sims C, Dimitri K, Manfrinetti P, Gofryk K, Oppeneer P M, and Neupane M 2021 *Phys. Rev. B* **104** L161115

[56] Wang Q, Neubauer K J, Duan C, Yin Q, Fujitsu S, Hosono H, Ye F, Zhang R, Chi S, Krycka K, Lei H, and Dai P 2021 *Phys. Rev. B* **103** 014416

[57] Gao L, Shen S, Wang Q, Shi W, Zhao Y, Li C, Cao W, Pei C, Ge J-Y, Li G, Li J, Chen Y, Yan S, and Qi Y 2021 *Appl. Phys. Lett.* **119** 092405

[58] Kabir F, Filippone R, Dhakal G, Lee Y, Poudel N, Casey J, Sakhya A P, Regmi S, Smith R, Manfrinetti P, Ke L, Gofryk K, Neupane M, and Pathak A K 2022 *Phys. Rev. Mater.* **6** 064404

[59] Zhou H, Shi M, Huang Y, Ma W, Xu X, Wang J, and Jia S 2023 *Phys. Rev. Mater.* **7** 024404

[60] Ishikawa H, Yajima T, Kawamura M, Mitamura H, and Kindo K 2021 *J. Phys. Soc. Jpn.* **90** 124704

[61] Pokharel G, Teicher S M L, Ortiz B R, Sarte P M, Wu G, Peng S, He J, Seshadri R, and Wilson S D 2021 *Phys. Rev. B* **104** 235139

[62] Peng S, Han Y, Pokharel G, Shen J, Li Z, Hashimoto M, Lu D, Ortiz B R, Luo Y, Li H, Guo M, Wang B, Cui S, Sun Z, Qiao Z, Wilson S D, and He J 2021 *Phys. Rev. Lett.* **127** 266401

[63] Rosenberg E, DeStefano J M, Guo Y, Oh J S, Hashimoto M, Lu D, Birgeneau R J, Lee Y, Ke L, Yi M, and Chu J H 2022 *Phys. Rev. B* **106** 115139

[64] Zhang X, Liu Z, Cui Q, Guo Q, Wang N, Shi L, Zhang H, Wang W, Dong X, Sun J, Dun Z, and Cheng J 2022 *Phys. Rev. Mater.* **6** 105001

[65] Lee J and Mun E 2022 *Phys. Rev. Mater.* **6** 083401

[66] Hu Y, Wu X, Yang Y, Gao S, Plumb N C, Schnyder A P, Xie W, Ma J, and Shi M 2022 *Sci. Adv.* **8** eadd2024

[67] Guo K, Ye J, Guan S, and Jia S 2023 *Phys. Rev. B* **107** 205151

[68] Arachchige H W S, Meier W R, Marshall M, Matsuoka T, Xue R, McGuire M A, Hermann R P, Cao H, and Mandrus D 2022 *Phys. Rev. Lett.* **129** 216402

[69] Zhang X, Hou J, Xia W, Xu Z, Yang P, Wang A, Liu Z, Shen J, Zhang H, Dong X, Uwatoko Y, Sun J, Wang B, Guo Y, and Cheng J 2022 *Materials* **15** 7372

[70] Kim D W, Liu S, Wang C, Nam H W, Pokharel G, Wilson S D, Cho J H, and Moon S J 2023 *Phys. Rev. B* **108** 205118

[71] Mozaffari S, Meier W R, Madhogaria R P, Peshcherenko N, Kang S H, Villanova J W, Arachchige H W S, Zheng G, Zhu Y, Chen K-W, Jenkins K, Zhang D, Chan A, Li L, Yoon M, Zhang Y, and Mandrus D G 2024 *Phys. Rev. B* **110** 035135

[72] Korshunov A, Hu H, Subires D, Jiang Y, Calugaru D, Feng X, Rajapitamahuni A, Yi C, Roychowdhury S, Vergniory M G, Strempfer J, Shekhar C, Vescovo E, Chernyshov D, Said A H, Bosak A, Felser C, Bernevig B A, and Blanco-Canosa S 2023 *Nat. Commun.* **14** 6646

[73] DeStefano J M, Rosenberg E, Peek O, Lee Y, Liu Z, Jiang Q, Ke L, and Chu J H 2023 *npj Quantum Mater.* **8** 65

[74] Hu Y, Ma J, Li Y, Jiang Y, Gawryluk D J, Hu T, Teyssier J, Multian V, Yin Z, Xu S, Shin S, Plokhikh I, Han X, Plumb N C, Liu Y, Yin J X, Guguchia Z, Zhao Y, Schnyder A P, Wu X, Pomjakushina E, Hasan M Z, Wang N, and Shi M 2024 *Nat. Commun.* **15** 1658

[75] Gu Y, Ritz E T, Meier W R, Blockmon A, Smith K, Madhogaria R P, Mozaffari S, Mandrus D, Birol T, and Musfeldt J L 2023 *npj Quantum Mater.* **8** 58

[76] Hu T, Pi H, Xu S, Yue L, Wu Q, Liu Q, Zhang S, Li R, Zhou X, Yuan J, Wu D, Dong T, Weng H, and Wang N 2023 *Phys. Rev. B* **107** 165119

[77] Cheng S, Ren Z, Li H, Oh J S, Tan H, Pokharel G, DeStefano J M, Rosenberg E, Guo Y, Zhang Y, Yue Z, Lee Y, Gorovikov S, Zonno M, Hashimoto M, Lu D, Ke L, Mazzola F, Kono J, Birgeneau R J, Chu J H, Wilson S D, Wang Z, Yan B, Yi M, and Zeljkovic I 2024 *npj Quantum Mater.* **9** 14

[78] Hu H, Jiang Y, Călugăru D, Feng X, Subires D, Vergniory M G, Felser C, Blanco-Canosa S, and Bernevig B A 2023 *Phys. Rev. B* **111** 054113

[79] Guguchia Z, Gawryluk D J, Shin S, Hao Z, Mielke Iii C, Das D, Plokhikh I, Liborio L, Shenton J K, Hu Y, Sazgari V, Medarde M, Deng H, Cai Y, Chen C, Jiang Y, Amato A, Shi M, Hasan M Z, Yin J X, Khasanov R, Pomjakushina E, and Luetkens H 2023 *Nat. Commun.* **14** 7796

[80] Tuniz M, Consiglio A, Puntel D, Bigi C, Enzner S, Pokharel G, Orgiani P, Bronsch W, Parmigiani F, Polewczyk V, King P D C, Wells J W, Zeljkovic I, Carrara P, Rossi G, Fujii J, Vobornik I, Wilson S D, Thomale R, Wehling T, Sangiovanni G, Panaccione G, Cilento F, Di Sante D, and Mazzola F 2023 *Commun. Mater.* **4** 103

[81] Liu S, Wang C, Yao S, Jia Y, Zhang Z, and Cho J H 2024 *Phys. Rev. B* **109** L121103

[82] Cao S, Xu C, Fukui H, Manjo T, Dong Y, Shi M, Liu Y, Cao C, and Song Y 2023 *Nat. Commun.* **14** 7671

[83] Yi C, Feng X, Mao N, Yanda P, Roychowdhury S, Zhang Y, Felser C, and Shekhar C 2024 *Phys. Rev. B* **109** 035124

[84] Kang S H, Li H, Meier W R, Villanova J W, Hus S, Jeon H, Arachchige H W S, Lu Q, Gai Z, Denlinger J, Moore R, Yoon M, and Mandrus D 2023 arXiv:2302.14041 [cond-mat.str-el]

[85] Tan H and Yan B 2023 *Phys. Rev. Lett.* **130** 266402

[86] Pokharel G, Ortiz B R, Kautzsch L, Gomez Alvarado S J, Mallayya K, Wu G, Kim E A, Ruff J P C, Sarker S, and Wilson S D 2023 *Phys. Rev. Mater.* **7** 104201

[87] Meier W R, Madhogaria R P, Mozaffari S, Marshall M, Graf D E, McGuire M A, Arachchige H W S, Allen C L, Driver J, Cao H, and Mandrus D 2023 *J. Am. Chem. Soc.* **145** 20943

[88] Romaka L, Stadnyk Y, Romaka V V, Demchenko P, Stadnyshyn M, and Konyk M 2011 *J. Alloy. Compd.* **509** 8862

[89] Zeng X Y, Wang H, Wang X Y, Lin J F, Gong J, Ma X P, Han K, Wang Y T, Dai Z Y, and Xia T L 2024 *Phys. Rev. B* **109** 104412

[90] Pokharel G, Ortiz B, Chamorro J, Sarte P, Kautzsch L, Wu G, Ruff J, and Wilson S D 2022 *Phys. Rev. Mater.* **6** 104202

[91] Kong X, Tao Z, Zhang R, Xia W, Chen X, Pei C, Ying T, Qi Y, Guo Y, Yang X, and Li S 2024 *Chin. Phys. Lett.* **41** 047503

[92] Ding J, Zhao N, Tao Z, Huang Z, Jiang Z, Yang Y, Cho S, Liu Z, Liu J, Guo Y, Liu K, Liu Z, and Shen D 2023 *J. Phys.: Condens. Matter* **35** 405502

[93] Ortiz B R, Meier W R, Pokharel G, Chamorro J, Yang F, Mozaffari S, Thaler A, Gomez Alvarado S J, Zhang H, Parker D S, Samolyuk G D, Paddison J A M, Yan J, Ye F, Sarker S, Wilson S D, Miao H, Mandrus D, and McGuire M A 2025 *J. Am. Chem. Soc.* **147** 5279

[94] Yang F Z, Huang X, Tan H, Kundu A, Kim S, Thinel M, Ingham J, Rajapitamahuni A, Cai Y Q, Nelson C, Vescovo E, Meier W R, Mandrus D, Ortiz B R, Pasupathy A N, Yan B, and Miao H 2025 *Phys. Rev. B* **112** 245113

[95] Giannozzi P, Baroni S, Bonini N, Calandra M, Car R, Cavazzoni C, Ceresoli D, Chiarotti G L, Cococcioni M, Dabo I, Dal Corso A, de Gironcoli S, Fabris S, Fratesi G, Gebauer R, Gerstmann U, Gougoussis C, Kokalj A, Lazzeri M, Martin-Samos L, Marzari N, Mauri F, Mazzarello R, Paolini S, Pasquarello A, Paulatto L, Sbraccia C, Scandolo S, Sclauzero G, Seitsonen A P, Smogunov A, Umari P, and Wentzcovitch R M 2009 *J. Phys.: Condens. Matter* **21** 395502

[96] Vanderbilt D 1990 *Phys. Rev. B* **41** 7892

[97] Perdew J P, Burke K, and Ernzerhof M 1996 *Phys. Rev. Lett.* **77** 3865

[98] Grimme S, Antony J, Ehrlich S, and Krieg H 2010 *J. Chem. Phys.* **132** 154104

[99] Baroni S, de Gironcoli S, Dal Corso A, and Giannozzi P 2001 *Rev. Mod. Phys.* **73** 515

[100] Allen P B and Dynes R C 1975 *Phys. Rev. B* **12** 905

[101] Jain A, Hautier G, Ong S P, Moore C J, Fischer C C, Persson K A, and Ceder G 2011 *Phys. Rev. B* **84** 045115

[102] Jain A, Ong S P, Hautier G, Chen W, Richards W D, Dacek S, Cholia S, Gunter D, Skinner D, Ceder G, and Persson K A 2013 *APL Mater.* **1** 011002

[103] Sun W, Dacek S T, Ong S P, Hautier G, Jain A, Richards W D, Gamst A C, Persson K A, and Ceder G 2016 *Sci. Adv.* **2** e1600225

[104] Zeller R 2006 *Comput. Nanoscience* **31** 419

[105] Shi L T, Si J G, Liang A, Turnbull R, Liu P F, and Wang B T 2023 *Phys. Rev. B* **107** 184503

[106] Si J G, Lu W J, Wu H Y, Lv H Y, Liang X, Li Q J, and Sun Y P 2020 *Phys. Rev. B* **101** 235405

[107] Si J G, Lu W J, Sun Y P, Liu P F, and Wang B T 2022 *Phys. Rev. B* **105** 024517

[108] Yan L, Ku R, Si J G, Liu P F, Gao H, Zhou L, and Wang B T 2024 *Phys. Rev. B* **109** 134502

[109] Pickard C J and Needs R J 2007 *Nat. Phys.* **3** 473

[110] Keimer B, Kivelson S A, Norman M R, Uchida S, and Zaanen J 2015 *Nature* **518** 179

[111] Liu Y, Shao D F, Li L J, Lu W J, Zhu X D, Tong P, Xiao R C, Ling L S, Xi C Y, Pi L, Tian H F, Yang H X, Li J Q, Song W H, Zhu X B, and Sun Y P 2016 *Phys. Rev. B* **94** 045131

[112] Li M, Wang Q, Wang G, Yuan Z, Song W, Lou R, Liu Z, Huang Y, Liu Z, Lei H, Yin Z, and Wang S 2021 *Nat. Commun.* **12** 3129

[113] Zhang S Y, Zhao P, Cheng Z H, Li R W, Sun J R, Zhang H W, and Shen B G 2001 *Phys. Rev. B* **64** 212404

[114] Schobinger-Papamantellos P, Rodríguez-Carvajal J, and Buschow K H J 2016 *J. Magn. Magn. Mater.* **408** 233